Asociación Argentina
de Mecánica Computacional

Mecánica Computacional Vol XXXI, págs. 85-112 (artículo completo)
Alberto Cardona, Paul H. Kohan, Ricardo D. Quinteros, Mario A. Storti (Eds.)
Salta, Argentina, 13-16 Noviembre 2012

NUMERICAL SIMULATION OF BUBBLY TWO-PHASE FLOW USING EULERIAN-EULERIAN MODEL

Santiago F. Corzo[a], Santiago Márquez Damián[a], Damian Ramajo[a] and Norberto M. Nigro[a]

[a]*International Center for Computational Methods in Engineering (CIMEC), INTEC-UNL/CONICET, Güemes 3450, Santa Fe, Argentina, santiagofcorzo@gmail.com, http://www.cimec.org.ar*

Keywords: Numerical simulation, Two-Fluid model, One-dimensional model, OpenFOAM®

Abstract. An accurate prediction of void generation and phase distribution on heat transfer under sub-cooled boiling regime is required in many industrial and laboratory applications. In this paper a one-dimensional code was implemented in order to study the mass and heat transfer amount phases during high heat transfer in water-steam systems. To obtain a well-postulated model, in a first step it was implemented a one-dimensional Eulerian-Eulerian two-fluid model. Attention was focused on the interfacial momentum exchange between phases caused by drag efforts. The two-fluid model implemented was generated following the solvers and libraries implemented on CFD OpenFOAM® code due to its full access, easy solver generation and modification. Finally, a mechanistic model from literature to predict sub-cooled boiling and bulk condensation is implemented and assessed with experimental data. This paper presents the constitutive relations implemented and highlighting the mechanistic model for mass exchange prediction.

1 INTRODUCTION

Subcooled boiling flow and associated heat transfer are encountered in many industrial applications. Particularly, in nuclear power reactors this phenomena affects the neutron moderation characteristics and implicitly the reactivity response of the system, just as flow instabilities. Two-Phase Eulerian models on subcooled boiling regime have been studied during the last 50 years. Much efforts have been applied to understand the subcooled boiling through one-dimensional empirical correlations models ((Levy, 1967), (Jens and Lottes, 1951), (Saha and Zuber, 1974), and (Thom, 1966)). All these models do not take into account thermal and hydrodynamics properties variations. In addition, they fail to describe a complete fluid regime and, to this date, they have not been employed in CFD applications. Moreover, these models do not allow the calculation of local parameters that perform a well description of the phenomenon. RPI (Rensselaer Polytechnic Institute) wall boiling based on local parameters (such as evaporation rate, bubble departure frequency, etc) developed by (Kurul and Podowski, 1991) has been used without any difficult in both CFD and one-dimensional problems.

The most applied approach to modeling separated flow is the Eulerian two-phase model and was used in the present research. This is based on assumptions of interface exchange, one pressure to both phases, and different continuous and dispersed velocities. The momentum interaction between both phases is phenomenologically missed by the assumptions proposed above. This is analyzed by empirical correlations based on experimental results.

Furthermore, is well know that, even though the implemented model has been widely accepted, an inherently non-hyperbolic and non-conservative ill-posed problem arises from the mathematical point of view (Issa and Kempf, 2003).

This drawback occurs even for the model hypothetical assumptions (i.e., an incompressible and inviscid model), this occurs by the lack of some physical properties as well as the appearance of complex eigenvalues (loss of hyperbolicity). The characteristics values analysis is not done in this paper. In these sense, special techniques were applied in order to obtain stable results. Among these, staggered grid were used to add numerical diffusion. Include additional interfacial terms in the momentum equation (i.e., virtual mass force) can achieve a stability equation system (Hwang, 2003).

In the present paper, a one-dimensional six-equation two-phase model are described to modeling the hydrodynamic and thermal behavior. Results was compared with classical benchmark cases available in the literature, finding excellent agreement with both experimental data.

2 MATHEMATICAL FORMULATION

The basic equations used in the present numerical research of two-phase flow are based on Euler-Euler model for a continuous liquid phase a and a dispersed bubbles phase b. This widely studied model in the scientific literature has been developed by different authors throughout the years((Ishii and Hibiki), (Evje and Fjelde, 2002)). The specific formulation to solve a two-phase flow is two sets of conservation equations for the balance of mass, momentum and energy for each of the phases. The formulation is focused on one-dimensional flows inside pipes of constant cross section. The continuity equation, assuming incompressibility of each phases can

be written as:

$$\frac{\partial \alpha}{\partial t} + \nabla \cdot (\alpha U_a) = \frac{E_{rate} - C_{rate}}{\rho_a} \tag{1}$$

where α_a denote the phase fraction of a, ρ_a is the density of the material, and U_a is the phase velocity. The scalar values E_{rate} and C_{rate} represent the evaporation and condensation rate per unit volume respectively. Both values are regarded as constant source terms. The conservation momentum equation is:

$$\frac{\partial(\alpha U_a)}{\partial t} + \nabla \cdot (\alpha U_a U_a) = -\nabla \cdot (\frac{\alpha}{\rho_a}(\tau_a + R_a)) - \frac{\alpha}{\rho_a}\nabla p_a + \alpha g + \frac{M_a}{\rho_a} + \frac{C_{rate}U_b - E_{rate}U_a}{\rho_a} \tag{2}$$

$$\frac{\partial(\beta U_b)}{\partial t} + \nabla \cdot (\beta U_b U_b) = -\nabla \cdot (\frac{\beta}{\rho_b}(\tau_b + R_b)) - \frac{\beta}{\rho_b}\nabla p_b + \beta g + \frac{M_b}{\rho_b} + \frac{E_{rate}U_a - C_{rate}U_b}{\rho_b} \tag{3}$$

here, both τ_a and τ_b are the laminar stress tensor of phase a and b respectively, R_a is the phase Reynols stress tensor, p is the pressure, and $M_{a,b}$ is the interfacial force per unit volume and will be the object of specific study in next sections. The last is the gain or loss of momentum due to phase change. The laminar stress tensor is defined for each phase ϕ, as

$$\tau_\phi = -\rho_\phi \nu_\phi [\nabla U_\phi + \nabla^T U_\phi] + \frac{2}{3}\rho_\phi \nu_\phi (\nabla \cdot U_\phi) I \tag{4}$$

where ν_ϕ is the molecular kinematic viscosity of the fluid constituting phase ϕ, and I is the identity matrix. The phase Reynolds stress tensor is given by

$$R_\phi = -\rho_\phi \nu_{\phi,t} [\nabla U_\phi + \nabla^T U_\phi] + \frac{2}{3}\rho_\phi \nu_{\phi,t} (\nabla \cdot U_\phi) I + \frac{2}{3}\rho_\phi \kappa_{\phi,t} I \tag{5}$$

Where $\kappa_{\phi,t}$ is the phase kinematic energy, and $\nu_{\phi,t}$ is the phase turbulent kinematic viscosity. The following simplifications are proposed for these equations: The turbulence parameters and the Reynolds stresses are neglected since the one-dimensional model only retains the component associated with axial diffusion $\nabla \cdot (\frac{\alpha}{\rho_a}\tau_a)$. These effects are small compared to the axial convective flow of momentum $\nabla \cdot (\alpha U_a U_a)$. This does not mean that turbulence effect are completely neglected, the more significant radial or transverse turbulent diffusion effect are included within wall friction correlations if it is necessary. Another approximation is to assume the both phasic pressure p is equal. The interfacial pressure are also assumed equal to the phasic pressures as well (Shieh et al.).

Under subcooled conditions the water-steam flow energy equation is solved for only liquid phase, while vapor is assumed to be saturated everywhere (Kurul and Podowski, 1991). It would be irrelevant to solve an energy equation for the gaseous phase under these conditions.

The continuous phase energy equation written in terms of specific enthalpy has the following form:

$$\frac{\partial(\beta h_b)}{\partial t} + \nabla \cdot (\beta h_b U_b) = -\frac{1}{\rho_b}\nabla \cdot (\beta q_b) + \frac{\beta}{\rho_b}\frac{Dp}{Dt} + \frac{Erateh_{sat} - Crateh_b}{\rho_b} + \frac{q_W A_W}{\rho_b} \tag{6}$$

where q_b is the heat flux inside phase b, the last term of the right hand side is the heat flux q_W from the wall with contact area per unit of volume A_W. The internal heat flux is defined by the Fourier law:

$$q_b = \frac{\lambda_b}{C_p}\nabla h_b \tag{7}$$

here λ_b is thermal conductivity and C_p is the specific heat.

The phase continuity equation is rewritten to avoid degeneration of the model to single-phase case and to kept the phase fraction of each phase between zero and one. Thus, rewriting the phase velocity in terms of the relative mean and relative velocity (See http://openfoamwiki.net/index.php/BubbleFoam).

$$U_r = U_a - U_b; U = \alpha U_a + \beta U_b; \tag{8}$$

we find:

$$U_a = U + \beta U_r; \tag{9}$$

Substituting into the phase continuity equation

$$\frac{\partial \alpha}{\partial t} + \nabla \cdot (\alpha U) + \nabla \cdot (\alpha(1-\alpha)U_r) = 0 \tag{10}$$

The non-linear term in Eqn. 10 is iterativelly solved in a fully implicit manner provided a bounded solution for the phase fraction field.

The momentum equation is rewritten in non-conservative form to extract the volume fraction from the transport terms, leading to

$$\frac{\partial U_a}{\partial t} + \nabla \cdot (U_a U_a) + \nabla \cdot (\frac{\tau_a}{\rho_a}) + \frac{\nabla \alpha}{\alpha}(\frac{\tau_a}{\rho_a}) = -\frac{\nabla p}{\rho_a} + g + \frac{M_a}{\alpha \rho_a} \tag{11}$$

$$\frac{\partial U_b}{\partial t} + \nabla \cdot (U_b U_b) + \nabla \cdot (\frac{\tau_b}{\rho_b}) + \frac{\nabla \beta}{\beta}(\frac{\tau_b}{\rho_b}) = -\frac{\nabla p}{\rho_b} + g + \frac{M_b}{\beta \rho_b} \tag{12}$$

where the stress tensor is defined as in equation 4.

$$\frac{\partial U_a}{\partial t} + \nabla \cdot (U_a U_a) + \nabla \cdot (\nu_a \nabla U_a) + \nu_a \frac{\nabla \alpha}{\alpha}(\nabla U_a) = -\frac{\nabla p}{\rho_a} + g + \frac{M_a}{\alpha \rho_a} \tag{13}$$

$$\frac{\partial U_b}{\partial t} + \nabla \cdot (U_b U_b) + \nabla \cdot (\nu_b \nabla U_b) + \nu_b \frac{\nabla \beta}{\beta}(\nabla U_b) = -\frac{\nabla p}{\rho_b} + g + \frac{M_b}{\beta \rho_b} \tag{14}$$

2.1 Interfacial Momentum exchange

Different mechanisms of interfacial momentum transfer have been discussed for two-fluid models in the past. These by studying of dimensionless equation of motion and making comparisons with experimental results (Enwald et al., 1996). The total interfacial force acting between two phases arises from several independent physical effects:

$$M_a = -M_b = M^D + M^{SL} + M^{WL} + M^{VM} + M^{TD} \tag{15}$$

which represent drag force and non-drag forces (lift force, wall-lubrication force, virtual mass force and turbulence dispersion respectively) (Pellacani et al.).

2.1.1 Drag force

This force represents the resistance opposed to the motion of bubbles, drops and particles in the continuous fluid. Its direction is opposite of the bubbles's relative velocity. The following form is used to model interphase drag force acting on phase α due to phase β

$$M^D = C_{\alpha\beta}(U_b - U_a) = C_{\alpha\beta}(U_a - U_b) \tag{16}$$

where compute $C_{\alpha\beta}$ from the drag coefficient as follow:

$$C_{\alpha\beta} = \frac{3}{4}\alpha\beta(\beta\frac{C_{D,a}\rho_b}{d_a} + \alpha\frac{C_{D,b}\rho_a}{d_b})|U_r| \tag{17}$$

where d_a and d_b are the phase particle diameters, and $C_{D,a}$ and $C_{D,b}$ are the drag coefficients computed with respect to each phase. Many empirical and semi-empirical equations have been proposed to approximate the effect of drag forces acting in experimental or analytical conditions of bubble or drops around other fluid (Clift et al., 1978). Some of these are Schiller and Naumman (Schiller and Naumann, 1933), Wen Yu drag model (Gidaspow, 1994), Ishii-Zuber drag model (Ishii and Zuber, 1979).

On dispersed multiphase flow at low particle Reynolds number, the drag coefficient for flow past spherical particles may be computed analytically under Stokes' law.

$$C_D = \frac{24}{Re_\phi}, Re << 1 \tag{18}$$

where particle Reynolds number to phase ϕ is computed as:

$$Re_\phi = \frac{|U_\phi| d_\phi}{\nu_\phi} \tag{19}$$

For particles Reynolds numbers sufficiently large, the drag coefficient becomes independent of Reynolds number:

$$C_D = 0,44, 1000 <= Re < 1,5 \times 10^5 \tag{20}$$

In the transitional region between $0,1 <= Re < 1000$ for spherical particles, both viscous and inertial effect are important. Hence, the drag coefficient is function of Reynolds number. Several empirical correlations are available for spherical particles. The best choose is **Schiller-Naumman drag coefficient model** bounded for the constant value $0,44$:

$$C_D = \max\left(\frac{24}{Re_\phi}(1 + 0.15Re_\phi^{0.687}), 0.44\right) \tag{21}$$

The Following section describe the non-drag forces:

2.1.2 Shear-Induced lift force

The lift force (or shear-induced Lift Force) acting on a dispersed phase β passing by a continuous phase α shear field. Mainly acting in the lateral direction. The lift force plays an important role and has a large effect on the radial distribution of bubbles. This is given by (Drew and Lahey Jr, 1987):

$$M^{SL} = \alpha\beta(\beta\rho_b C_{L,a} + \alpha\rho_a C_{L,b})U_r \times (\nabla \times U) \tag{22}$$

where $C_{L,\phi}$ is the non-dimensional lift coefficient estimated by a empirical correlation. This contribution to the interfacial momentum term is neglected due to $U_r \times (\nabla \times U)$ vanishes for one-dimensional models.

2.1.3 Wall-Induced lift force

Due to no-slip condition at the wall, the bubbles near the wall are affected by the Wall Lift Force (or Wall-Lubrication force) towards the center of the bulk and prevent attaching on the wall. This force acts in lateral direction away from the wall to avoid accumulation of bubbles on the wall. This effect is neglected for one-dimensional models.

2.1.4 Virtual mass Force

Virtual mass force or added mass force is produced from the relative acceleration of one phase respect to the other. For this reason this force is neglected when running steady state problems. The force is calculated by the following widely-used correlation.

$$M^{VM} = \alpha\beta C_{VM}\rho_b\left(\frac{DU_b}{dt} - \frac{DU_a^b}{dt}\right) \tag{23}$$

where C_{VM} is the virtual mass coefficient, and U_a^b is the local liquid velocity evaluated at the bubble center position.

2.2 Wall Friction Momentum Models

The pressure drop in two-phase flow is closely related to the flow pattern, for this reason, numerous researchers have been concerned with local pressure drop in well-characterized two-phase flow patterns. Several phenomenological models were developed for different flow patterns (e.g., annular, slug, and stratified flows). In these specific models difficulties arise associated to the uncertainties on the flow regime transitions (Ghiaasiaan, 2008).

The pressure drop in two-phase flow has often been predicted by empirical correlations that remain the most widely applied method. These additional expressions for the frictional pressure drop are included on momentum equations. These represent the neglected effect of transversal stress tensor acts on the walls of the pipe. One possibility is to use the homogeneous flow models, but in that case, the equations reduce to drift or mixture models of one momentum equations. This option are a powerful tool because performs reasonably well in mixed configurations (e.g., dispersed bubbly) (Wallis, 1969). Another choice is Martinelli-Nelson that is related to separated flow regime.

On two-phase models (e.g., liquid-gas configuration) we know how to compute the pressure gradient which would occur if the fluid were flowing alone in the pipe ($\frac{dp}{dz}_f$ and $\frac{dp}{dz}_g$). The pressure gradient on the fluid denoted by ($\frac{dp}{dz}$) is defined as the frictional pressure drop in the pipe. Most empirical correlations are based on two-phase multiplier approach denoted by the symbol ϕ^2 with appropriated subscripts (e.g., ${\phi_{f0}}^2$ to the ratio between the frictional pressure drop for the two-phase flow respect the to the frictional pressure drop for related single-phase). Since the strong dependency of the pressure drop with the flow regime for both liquid and gas, four different combinations are possible. The individual phase pressure drops are calculated

by apportioning of the two-phase pressure drops ($\frac{dp}{dz}$). One possibility for this is the Lockhard-Martinelli correlation or Chisholm technique improved from Lockhard-Martinelli model.

2.3 Lockhard-Martinelli empirical correlation

The Lockhard-Martinelli (L-M) approach computes the overall two-phase friction pressure drop in terms of the liquid-alone wall friction pressure drop [see equation 24] and in terms of the gas-alone wall friction pressure drop $\frac{dp}{dz}_g$:

$$(\frac{dp}{dz})_{2\phi} = {\phi_f}^2 (\frac{dp}{dz})_f \tag{24}$$

$$(\frac{dp}{dz})_{2\phi} = {\phi_g}^2 (\frac{dp}{dz})_g \tag{25}$$

where ϕ_f and ϕ_g are the liquid and gas two-phase multipliers respectively. L-M assumes that the two-phase multipliers are related through the Martinelli parameter defined as:

$$\chi^2 = \frac{(\frac{dp}{dz})_f}{(\frac{dp}{dz})_g} = \frac{{\phi_g}^2}{{\phi_f}^2} \tag{26}$$

Lockhart and Martinelli correlated the liquid and gas two-phase multipliers (${\phi_f}^2$ and ${\phi_g}^2$) as functions of χ. The Martinelli parameter represents the degree to which the two-phase mixture behaves as the liquid rather than as the gas.

Each frictional pressure drop ($\frac{dp}{dz}_f$ and $\frac{dp}{dz}_g$) depends on the flow regimes of the phases (viscous or turbulent) and it is discussed in the follow chapter.

Regarding to the liquid and gas two-phase multipliers (${\phi_f}^2$ and ${\phi_g}^2$) compute, algebraic correlations have been proposed based on the Lockhard-Martinelli approach. One of these was performed by Chisholm (Chisholm and Laird, 1958):

$${\phi_f}^2 = 1 + \frac{C}{\chi} + \frac{1}{\chi^2} \tag{27}$$

$${\phi_g}^2 = 1 + C \cdot \chi + \chi^2 \tag{28}$$

where C are computed as a function of both phases regimes(turbulent or viscous). The value of coefficient $C_{l,g}$ is defined by the subscripts turbulent t and viscous v for liquid l and gas phases: $C_{t,t} = 20$, $C_{v,t} = 12$, $C_{t,v} = 10$, $C_{v,v} = 5$.

Wallis (Wallis, 1969) proposed a very simple model where two-phase separated without interaction in two concentric cylinders is assumed. The pressure drop in both phases is calculated from single-phase flow theory. This analytical theory give the following expression:

$$(\frac{1}{{\phi_f}^2})^{1/n} + (\frac{1}{{\phi_g}^2})^{1/n} = 1 \tag{29}$$

where $n = 2$ for laminar flow, $n = 2,375$ to $2,5$ for turbulent flow analyzed on a basis of friction factor, and $n = 2.5$ to 3.5 for turbulent flow. Figure 1 compares the gas multiplier using L-M and (Wallis, 1969).

The Heat Transfer and Fluid Flow Service (HTFS) model (Claxton et al., 1972) propose the Baroczy correlation to calculate the two-phase multipliers (${\phi_f}^2$ and ${\phi_g}^2$). This correlation is

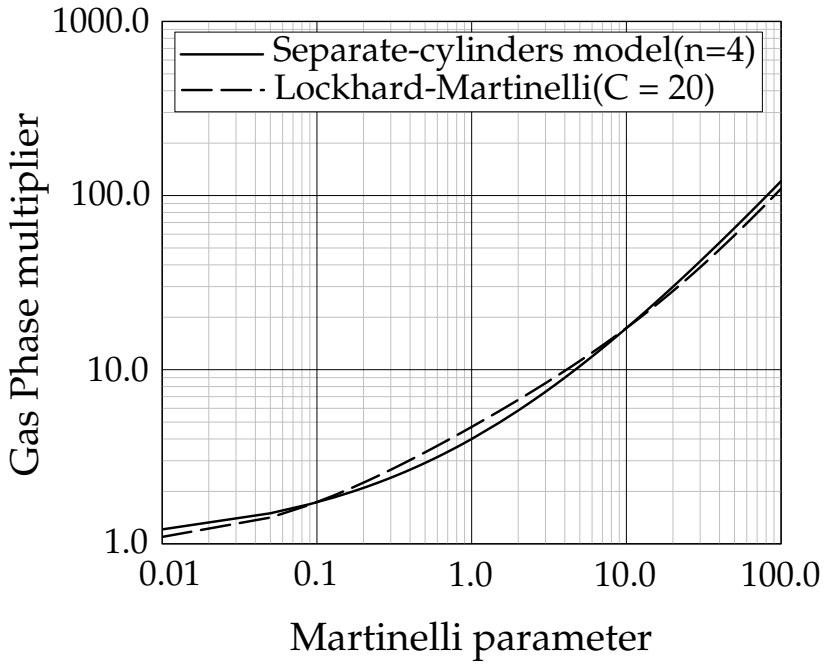

Figure 1: Two-phase multiplier ϕ_g to turbulent-turbulent flow

used over a broad ranges of phasic volume fractions, phasic flow rates and phasic flow regimes. This model compute the coefficients using L-M approach where the correlation coefficient C is expressed as:

$$C = -2 + (28 - 0,3G^{1/2}) \exp\left(-\frac{(log_{10}\Lambda + 2,5)^2}{2,4 - G(10^{-4})}\right) \tag{30}$$

where G is the total mass flow rate and Λ is the Baroczy dimensionless index defined as $\Lambda = \frac{\rho_g}{\rho_f}\left(\frac{\mu_f}{\mu_g}\right)^{0,2}$.

To compute the frictional pressure drop ($\frac{dp}{dz}$) in all models, combined the equation 24 through 26, and 28, then:

$$\left(\frac{dp}{dz}\right)_{2\phi} = {\phi_g}^2 \left(\frac{dp}{dz}\right)_g = \left(\frac{dp}{dz}\right)_g + C\left[\left(\frac{dp}{dz}\right)_f \cdot \left(\frac{dp}{dz}\right)_g\right]^{1/2} + \left(\frac{dp}{dz}\right)_f \tag{31}$$

In this work the friction pressure drop model based in terms of the two-phase friction multipliers was implemented. The Chisholm theoretical model (Chisholm and Laird, 1958) based on Lockhart-Martinelli was applied to obtain the individuals phases drop pressures. These wall shears can be defined from the overall frictional pressure drop and the parameter Z^2 as

$$\tau_f = \alpha \left(\frac{dp}{dz}\right)_{2\phi} \left(\frac{Z^2}{\beta + \alpha Z^2}\right) \tag{32}$$

$$\tau_g = \beta \left(\frac{dp}{dz}\right)_{2\phi} \left(\frac{1}{\beta + \alpha Z^2}\right) \tag{33}$$

where

$$Z^2 = \frac{\lambda_f \rho_f {U_f}^2 \frac{\beta_w}{\beta}}{\lambda_g \rho_g {U_g}^2 \frac{\alpha_w}{\alpha}} \tag{34}$$

These dependent flow regime variable allows to model the whole evaporation range. Here, α_w and β_w represent an estimated liquid and gas volume fraction in the wall respectively. For bubble regime the α_w and β_w are assumed as $\alpha_w = \alpha$ and $\beta_w = \beta$.

A comparison between Martinelli-Nelson, Lockhard-Martinelli, and a Homogeneous model is given in Figure 2(a) in terms of an adimensional number defined as the overall frictional pressure drop over alone-phase frictional pressure drop. Furthermore, 2(b) shows the independent frictional drop pressures gives by Lockhard-Martinelli for each phase. These results were obtained from (Wallis, 1969) test where a mixture flow (Water-air) is carried on a pipe of $0,197$" ($5,0038$ mm) and 1m of length, 1000 psi ($68,96$ bar) of pressure, the values were computed to $3,22 \times 10^6$ lb/h ft^2 = $4,3671 \times 10^3$ kg/s m^2.

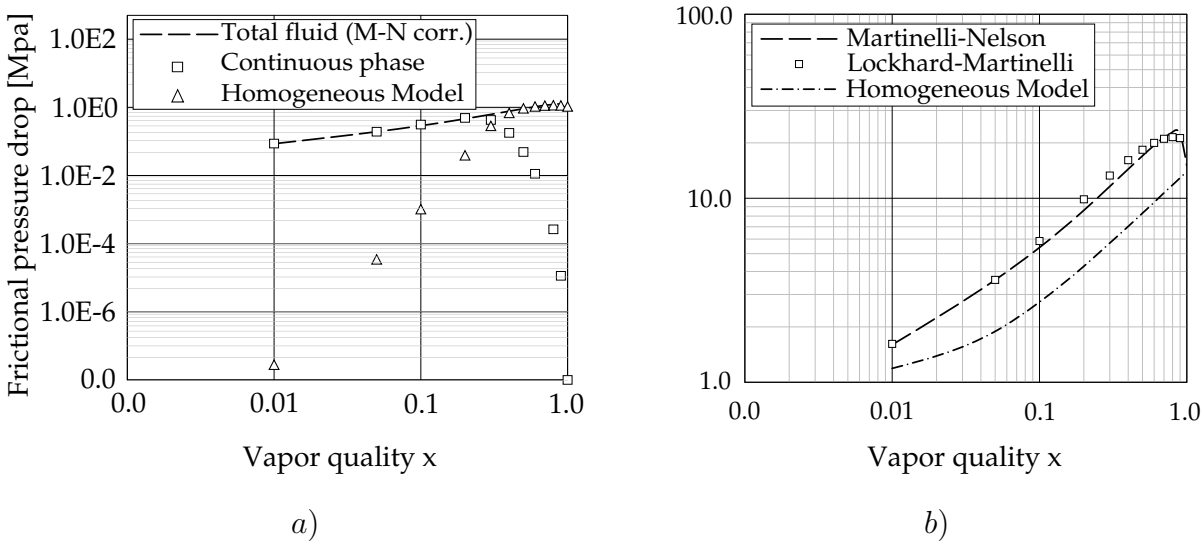

Figure 2: Frictional pressure drop models: a) Comparison between diferents models , b) Lockhard-Martinelli model

2.4 One-phase wall friction empirical correlation

The Darcy-Weisbach friction factor is evaluated from correlations as a function of Reynolds number according to the hydraulic regime. For laminar flow ($0 \leq Re < 2200$) the Darcy-Weisbach friction factor is calculated according to the equation of Hagen-Poiseuille:

$$\lambda_l = 64/Re \tag{35}$$

At turbulent flow conditions ($Re \geq 3000$), the equation of Colebrook (Cordes, 1969) can be used:

$$\frac{1}{\sqrt{\lambda_t}} = -2\log_{10}\left(\frac{2,15}{Re\sqrt{\lambda_t}} + 0,27\frac{r}{DH}\right) \tag{36}$$

where ε is r is the surface roughness and DH is hydraulic diameter.

Another turbulent friction factor is given by the Zigrang-Sylvester approximation (Lerchl and Austregesilo, 1995) to the Colebrook-White correlation, which is

$$\frac{1}{\sqrt{\lambda_t}} = -2\log_{10}\left[0,27\frac{r}{DH} + \frac{2,15}{Re}[1.14 - 2\log_{10}(\frac{r}{DH} + \frac{21.25}{Re^{0.9}})]\right] \tag{37}$$

The last model was implemented on `myTwoPhaseEulerFoam` solver. To avoid the discontinuity at transition region ($2200 \leq Re < 3000$) between laminar and turbulent flows, an interpolation equation was used in this zone:

$$\lambda_{lt} = \left(3.75 - \frac{8.250}{Re}\right)(\lambda_{t,3000} - \lambda_{l,2200}) + \lambda_{l,2200} \tag{38}$$

where $\lambda_{t,3000}$ is the turbulent friction factor at Reynold number of 3000, and $\lambda_{l,2200}$ is the laminar friction factor at Reynold number of 2200. Figure 3 shows this transition region to different wall roughness.

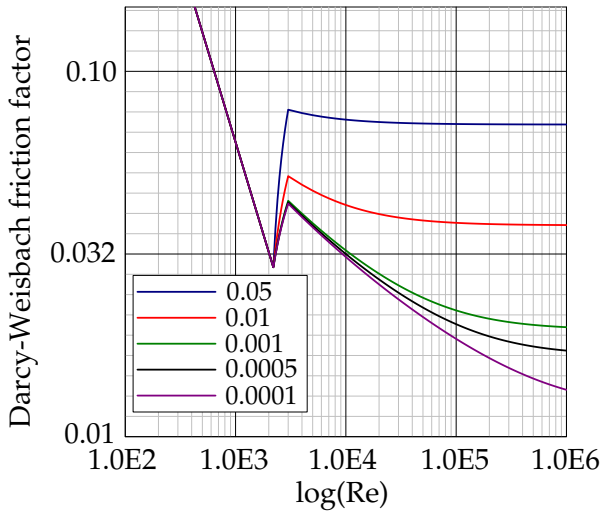

Figure 3: Darcy-Weisbach friction factor model

3 NUMERICAL IMPLEMENTATION

The Two-phase eulerian model is based on OpenFOAM® (Open Field Operation and Manipulation) suite solver `twoPhaseEulerFoam`. This software uses a finite volume discretization (Versteeg and Malalasekera, 2007), (Ferziger and Perić, 1999) and has free access to the code under the GNU-GPL license. The work of Jasak (Jasak, 1996) provides a description and implementation of the method especially in the OpenFOAM frame work.

The gauss' theorem was used to the spatial discretization of equations 10, 13 and 14. Temporal discretization to perform the temporal integration is a simple order backward-euler. Convection terms require the faces cell values (ϕ_f) to be calculated from the values in the cell centroid values (owner ϕ_P and neighbor ϕ_N cell), which is obtained using different convection differencing scheme. These operations produces an algebraic version of the transport partial differential equations (PDE):

$$a_P {\phi_P}^n + \sum a_N {\phi_N}^n = R_P \tag{39}$$

This equation can be expressed in matrix form as:

$$[A][x] = [b] \tag{40}$$

The PIMPLE (hybrid PISO/SIMPLE) algorithm is chosen for the pressure-velocity coupling. The standard PISO algorithms is not feasible for simulations of this kind of flows due to the stringent constraint on time step size imposed by PISO. For this purpose PIMPLE algorithm was applied. This hybrid coupling has better control convergence stability than PISO. A graphical representation of the solution loop procedure applied in the solver can be seen in Figure 4.

The PDE in equation 40 is represented in OpenFOAM® code using the classes of statics functions **finiteVolumeMethod** (**fvm**) and **finiteVolumeCalculus** (**fvc**). Both operators contain the differential operators (e.g.∇, ∇^2,and $\frac{\partial}{\partial t}$) to solve the transport variable on the PDE. The functions **fvm** calculate implicit derivatives to return a matrix object. Some **fvc** functions calculate explicit derivatives and other explicit calculations to return a geometric field (Guide, 2004).

The main advantage of OpenFOAM's source code solvers is its equation representation, whose syntax is really similar to the mathematical one. Following an present an example is presented to show this relatively ease syntax code on the mass transport equation **alphaEqn.H**.

alphaEqn.H

```
{
    surfaceScalarField phic("phic", phi);
    surfaceScalarField phir("phir", phia - phib);
    ...
    for (int acorr=0; acorr<nAlphaCorr; acorr++)
    {
        fvScalarMatrix alphaEqn
        (
            fvm::ddt(alpha)
          + fvm::div(phic, alpha, scheme)
          + fvm::div(-fvc::flux(-phir, beta, schemer), alpha, schemer)
```

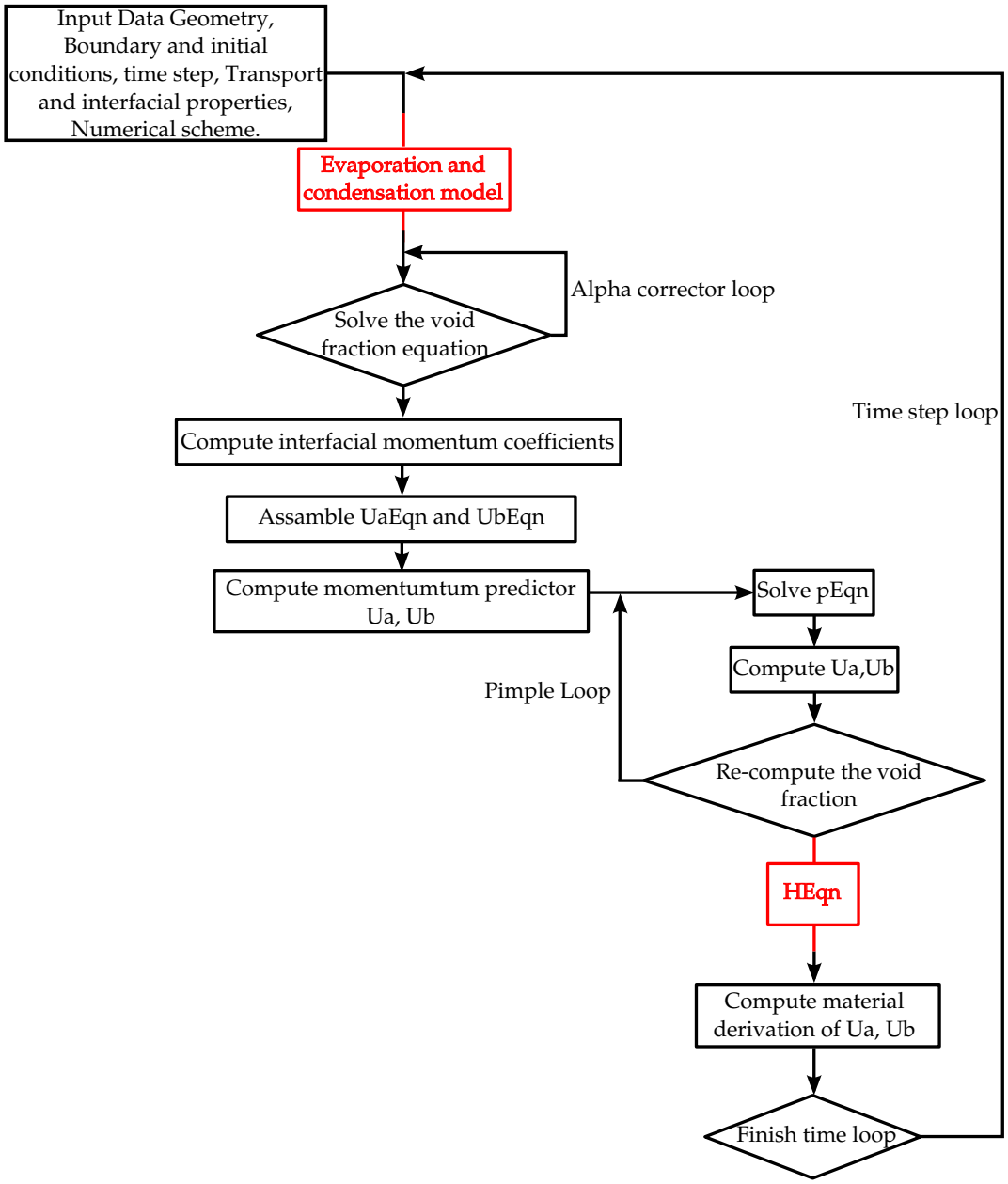

Figure 4: Detail of twoPhaseEulerFoam Model

```
        );
                                ...
        alphaEqn.relax();
        alphaEqn.solve();

        #include "packingLimiter.H"

        beta = scalar(1) - alpha;
                                ...                                    20
    }
}
rho = alpha*rhoa + beta*rhob;
```

Like the above source code, `twoPhaseEulerFoam` solver is already implemented in **OpenFOAM** software based on the scheme architecture that can be see on Figure 4.

The purpose of this paper is to develop the complete source code to solve one-dimensional two-phase problems. This is a successful alternative to simplify the mathematical complexity problem, and achieve good results on physical problems where the geometry is very simply (e.g. forced convection cooling on pipes).

To reach these objectives, the main operators **fvm** and **fvc** were implemented on **octave** as part of the octave-of suite(See http://code.google.com/p/octave-of/) and rated in a root file of the code. All these functions were implemented for one-dimensional flow. The main solver script calls the same operators and functions as `twoPhaseEulerFoam` to achieve the transition state solution.

Figure 4 shows the implementation of wall subcooled boiling model in `twoPhaseEulerFoam` based on (Kurul and Podowski, 1991). These models and their implementation will be described in more depth in the following sections.

3.1 Wall subcooled boiling model

The subcooled boiling phenomena occurs previews to the critical heat flux. The heat flux applied to the wall is too high to avoid the local evaporation on the nucleation sites, whereas the bulk flow is kept on subcooled single-phase conditions. The saturation temperature is exceeded only in the near-wall region. The mean temperature like as the bulk temperature is still bellow saturation condition. The steam bubbles are generated on the potential nucleation sites and departures the heated wall toward the core subcooled flow. The bubbles grow on the wall and leave it when achieve a critical bubble size. The model is detailed below in terms of a liquid phase l and a saturated steam phase g.

The model developed by Kurul and Podowski (Kurul and Podowski, 1991) define the wall partition based on the division of the total heat flux applied. This is separated in different terms: turbulent convection liquid, conduction quenching due to the departing bubbles and evaporation on the near-wall:

$$Q_{tot} = Q_{fc} + Q_q + Q_e \tag{41}$$

The single phase turbulent convection heat flux transfered to the subcooled liquid near the

wall $A1F$ is calculated by:

$$Q_{fc} = A1F \cdot h_{fc}(T_w - T_{l(nw)}) \tag{42}$$

where T_w is the wall temperature and $T_{l(nw)}$ is the liquid temperature near the wall. In the following section we describe the calculation of these variables. $A1F$ is the wall area fraction where the convection heat flux occur. The value of $A1F$ is the remaining part of the wall $A1F = 1 - A2F$. Where $A2F$ is the wall fraction area influenced by quenching. The wall heat transfer coefficient h_{fc} was computed by empirical correlations used by (Kurul and Podowski, 1991).

$$h_{fc} = St\rho_l Cp_l |U_l| \tag{43}$$

where the Stanton number is computed by another empirical correlation:

$$St = \frac{{\lambda_f}^2}{1 - 1,783\lambda_f} \tag{44}$$

the suggested fanning friction factor λ_f for pure liquid is

$$\lambda_f = \frac{1}{\frac{ln(\tilde{R}e\lambda_f)}{0,435} + 5.05} \tag{45}$$

and the constant $\tilde{R}e$ is computed by:

$$\tilde{R}e = \frac{3,2586 \times 10^{-4} |U_{l,bulk}|}{\nu_l} \tag{46}$$

The evaporation model is schematically shown in Figure 5. In a first step, the wall superheated ($T_{sup} = T_{wall} - T_{sat}$) is guessed assuming that the total heat flux is dedicated to single-phase convection [$Q_w = Q_{fc}$ and ($A1F = 1$)] with a temperature defined by ($T_{sub} = T_{sat} - T_l$) in the near-wall. At the end of chapter discuss about how to define the liquid temperature close to the wall from the mean value. The one-dimensional model misses the variables behavior on traversal section. For this, the temperature profile is not defined such as in CFD models.

$$T_{sup} = \frac{Q_w}{h_{fc}} - T_{sub} \tag{47}$$

Whit this temperature predictor the model performs the different model steps and compute the subcooled parameters. Under subcooled condition in the computational on each near-wall cell, the following parameters are computed: For bubble departure diameter d_w several correlations can be applied. At high subcooled boiling ($T_{sub} > 2K$) the (Unal, 1976) correlation was applied. In the present work, a modified (Unal, 1976) correlation by (BOREE et al.) was used.

$$d_w = \frac{2,42 \cdot 10^{-5} p^{0,705} A}{\sqrt{B\Phi}} \tag{48}$$

where the constant values A and B vary with wall temperature and material properties and:

$$\Phi = \begin{cases} \left(\frac{U_{l,bulk}}{0,61}\right)^{0,47} & \text{if } U_{l,bulk} > 0,61; \\ 1 & \text{if } U_{l,bulk} < 0,61 \end{cases}$$

In the other hand, for low subcooled boiling the Tolubinsky correlation (Tolubinsky and Kostanchuk, 1970) or linear interpolation was used.

$$d_w = 0,0014exp(-\frac{T_{sat} - T_l}{45}) \tag{49}$$

The surface density of active nucleation sites N depend mostly on the superheated potency.

$$N = (210T_{sup})^{1,805} \tag{50}$$

The bubble departure frequency can be estimated by the analytical results of (Ceumern-Lindenstjerna, 1997):

$$f = \sqrt{\frac{4(\rho_l - \rho_g)g}{3\rho_l d_w}} \tag{51}$$

The wall area fraction where evaporation occurs was estimated by Del Valle (Del Valle and Kenning, 1985) as function of the bubble detachment diameter:

$$A2F = \pi N {d_w}^2 \tag{52}$$

Whereas the convection heat flux dominates on the remaining part of the wall $A1F = 1 - A2F$. Once assessed all subcooled parameter the model describes the nucleate wall boiling process as the periodic releases of bubbles by each nucleation sites. This was computed by the nucleation site density. Thus, the mass flow evaporation ratio is:

$$Erate = \frac{\pi}{6} {d_w}^3 N f \rho_g \tag{53}$$

The quenching wall heat transfer coefficient was calculated based on analytical solutions by (Del Valle and Kenning, 1985):

$$h_q = \frac{2\lambda_l}{\sqrt{\frac{\pi}{f}\frac{\lambda_l}{\rho_l C p_l}}} \tag{54}$$

Finally, the Newton iterative loop (see figure 5) computes the total wall heat transfer:

$$Q_{tot} = Erate h_{lg} + (A1F h_{fc} + A2F h_q)(T_{sub} + T_{sup}) \tag{55}$$

where h_{lg} is the vaporization enthalpy and the first term is the total heat transfer by evaporation. With this values the wall temperature is re-computed to adjust its value with the total heat transfer.

When the steam bubbles move through the subcooled liquid, they condense, releasing the latent heat. For subcooled flow, the condensation only occurs away from the wall. The intefacial mass transfer related to condensation of vapor bubbles in the bulk is defined as:

$$Crate = \frac{h_c(T_{sat} - T_l)A_{lg}}{h_{lg}} \tag{56}$$

here h_{lg} is the evaporation enthalpy and A_{lg} is the interfacial area per unit volume. The heat transfer coefficient for condensation h_c was developed by Wolfert (Wolfert et al., 1978) assuming bubbles are at saturated conditions:

$$h_c = \rho_l C p_l \sqrt{\frac{\pi}{4}\frac{|U_g - |U_l|}{Ds}\frac{\lambda_l}{\rho_l C p_l}\frac{1}{\left(1+\frac{{\lambda_l}^t}{\lambda_l}\right)}} \tag{57}$$

where Ds is the bubble saturated diameter and ${\lambda_l}^t$ is the turbulent thermal conductivity assumed equal to λ_l for one-dimensional problems. The interfacial area per unit volume ai correspond to the area of the gas bubbles into the liquid. For spherical bubbles, A_{lg} is proportional to the void fraction and inversely proportional to the bubble diameter.

$$A_{lg} = 6\frac{\alpha}{Ds} \tag{58}$$

The issue refereed above, about the temperature description in near-wall region will be solved by empirical correlations for temperature and momentum variables. On the other hand the turbulent regime and the non-developed flow impedes this assignment. To this end, in future researches we propose different alternatives to approach the problem. The main alternative will be define an relationship between the main temperature computed by the enthalpy equation and a wall temperature defined easily by a theoretical study about evaporation flows.

In follow chapter we propose to use experimental test from Bartolomej (Bartolomej and Chanturiya, 1967) experimental test to compare the evaporation model applied into a complete steady state solution. So that, in appendix section we presents CFD numerical results using CFX software.

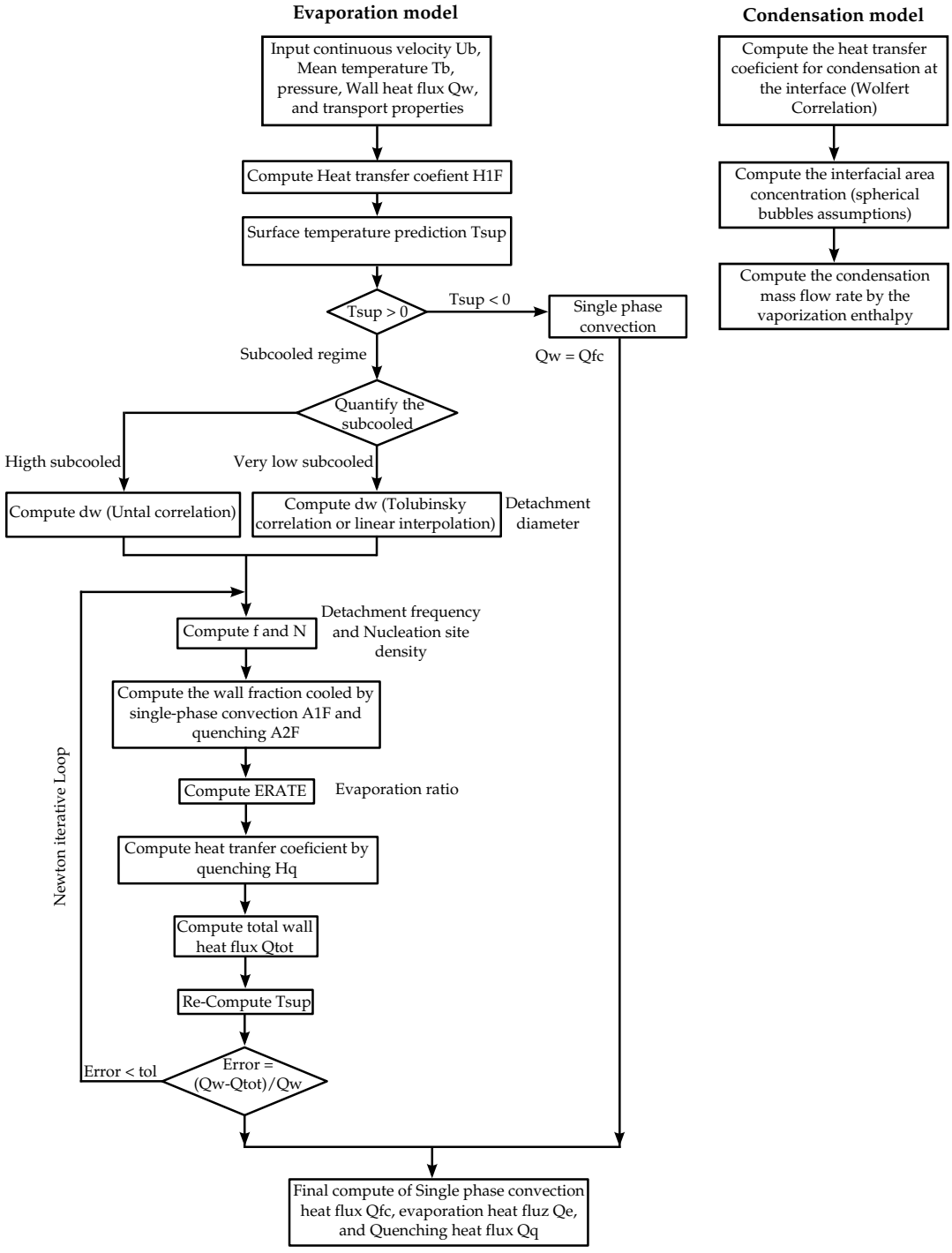

Figure 5: Detail of evaporation and condensation model

4 NUMERICAL BENCHMARKS

In this section we analyze the numerical benchmarks presented on the literature with the aim of study the behaviour of the code implemeted.

4.1 Water Faucet Test

The simplified physical phenomena where the separation of air and water by gravity in a vertical tube proposed by Ransom (Ransom and Mousseau, 1991) is a well-known benchmarks problem (Hewitt, 1983). The water Faucet problem has been extensively studied by several researchers to check the capability of the two-fluid models.

The test consists of a vertical tube of 12m length and 1m diameter. The pipe is assumed to be adiabatic and in the initial state is filled with a homogeneous two-phase mixture (air, water) of constant void fraction of $\alpha = 0,8$; The boundary and initial conditions are summarized on table 1 and the physical phenomenon is illustrated schematically in Figure 6.

The presented results have been achieved using a time step of (1×10^{-4} sec.) except cases that uses high order divergence scheme where the courant number limitation make impossible to use that time step. Simulations were carried out with three correctors of PIMPLE loop (`nCorrectors` = 3), two alpha correctors (`nAlphaCorr` = 2) and enables the alpha correction on last PIMPLE loop.

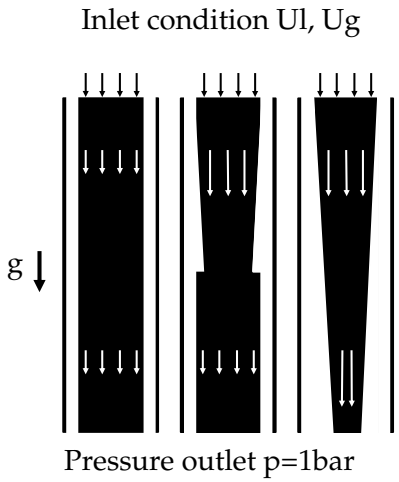

Figure 6: Detail of water faucet test

The numerical results obtained can be compared to the an analytical solution:

$$\begin{cases} \alpha = 1 - \frac{\beta \cdot v_{l,0}}{v_{l,0}}; \\ v_l = (v_{l,0}^2 + 2gx)^{1/2} \end{cases} \quad x < (v_{l,0}t + \tfrac{1}{2}gt^2)$$

and otherwise $\beta = 1 - \alpha$.

The water faucet assumes that interfacial momentum interaction are negligible. When the simulation starts ($t = 0$), a gravity field ($g = 9,8$ m/s^2) is applied and this causes the water

Table 1: Details of Water Faucet Problem

Geometric details			
Length (m)	12		
Diameter (m)	1		
Initial Conditions		**Boundary Conditions**	
$T(C)$	50	$T_{inlet}(C)$	50
$p(Pa)$	10^5	$p_{outlet}(Pa)$	10^5
α	0.8	α	0.8
$u_l(m/s)$	10	$u_{inlet,l}(m/s)$	10
$u_g(m/s)$	0	$u_{inlet,g}(m/s)$	0

column to accelerate. Due to the acceleration, a contact discontinuity propagates downwards until a steady state is reached when the discontinuity arrives at the outlet.

This problem was simulated with tree different meshes of 20, 120, 600 uniform lineal volume controls. In Figs. 9 a) and b) the numerical and analytical solutions for the void fraction and water velocity are shown at the instant ($t = 0.5$sec.).

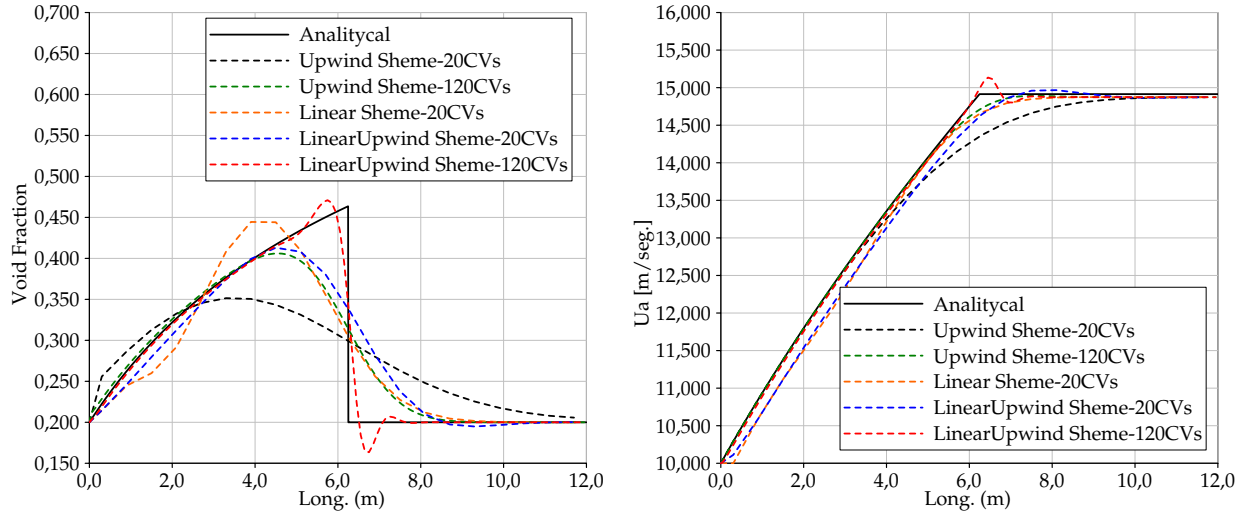

a) b)

Figure 7: Analytical and numerical comparison at ($t = 0.5seg.$) of water faucet case: a) Void Fraction, b) Liquid velocity

Figure 8 correspond to several times in which the discontinuity is still within the tube. Although agreement between numerical and analytical solutions in a transient state is not expected, these figures show that the velocity of propagation of the discontinuity is well reproduced. Besides, numerical solutions for water velocity and void fraction approach analytical values when the number of volume controls is increased, capturing the contact discontinuity very well.

The problem of well-posed boundary conditions is an essential question in the water faucet

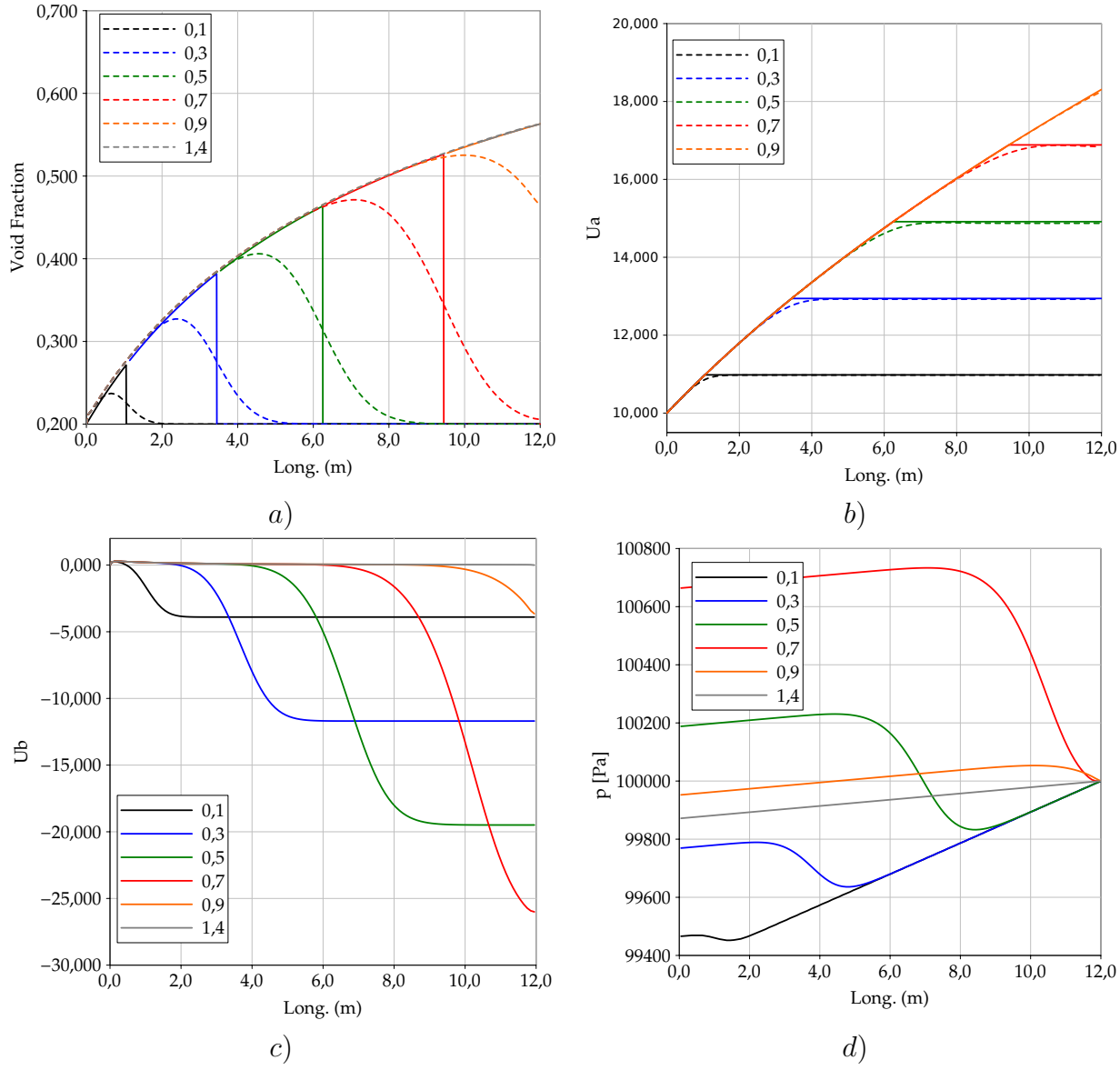

Figure 8: Analytical and numerical transient of water faucet case: a) Void Fraction, b) Liquid velocity, c) Gas velocity and d) pressure

test. An unconditionally well-posed problem is not achieved due to the fact that liquid and gas velocity are unequal and with opposite directions. For this reason, the numerical result shows instabilities that grow when the mesh size is refined (Morales-Ruiz et al., 2012).

Finally in Figure 9 shows the comparison between twoPhaseEulerFoam and octave mytwoPhaseEulerFoam emulator.

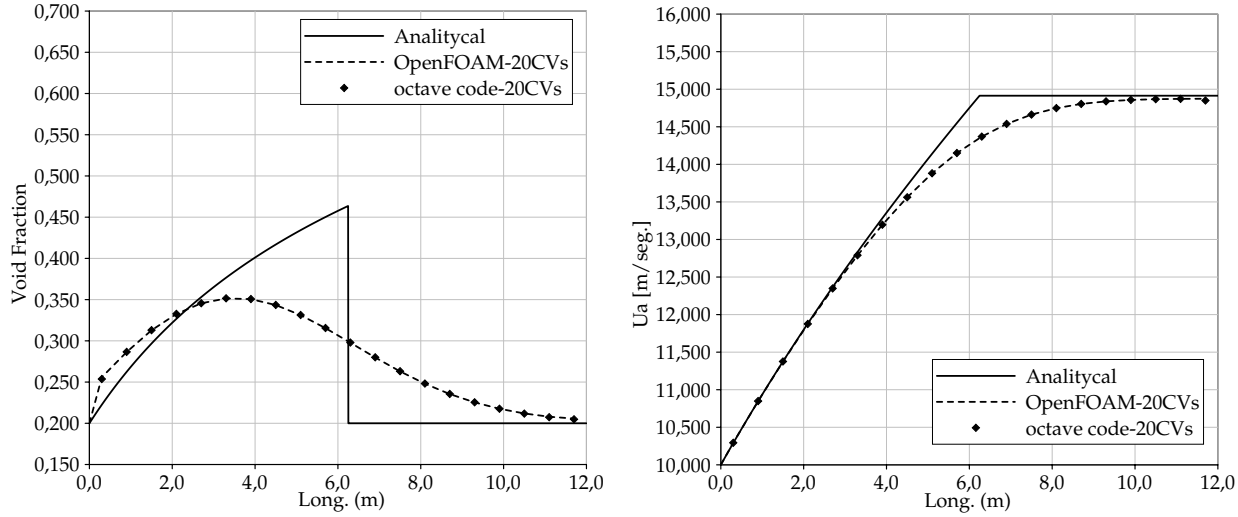

a) b)

Figure 9: Analytical and numerical comparison at ($t = 0.5seg.$) between myTwoPhaseEulerFoam and octave emulator to the water faucet case: a) Void Fraction, b) Liquid velocity

4.2 Horizontal particle transport

The particle transport is present in many industrial applications, for this reason we propose a simple test with analytical solution to validate the model in this problem. Figure 12 show a schematic representation of the physical problem. The test analyze the steady state solution for solid particles in a free stream of air. The problem allow us ascertain the drag force influence between continuous and dispersed phases. The analytical solution for dispersed phase velocity was developed by (Moukalled and Darwish, 2002):

$$\ln[\mathrm{U}_{b,inlet} - U_a] + \frac{U_{b,inlet}}{U_{b,inlet} - U_a} = \frac{3}{8}\frac{rho_b}{rho_a}\frac{Cd}{d_a}z + ln[U_{b,inlet} - U_{a,inlet}] + \frac{U_{b,inlet}}{U_{b,inlet} - U_{a,inlet}} \quad (59)$$

The test parameters are summarized on table 2 and the dispersed phase is modeled with particle radius of 1mm. The density relationship is $\rho_d/\rho_c = 2000$. The present results have been carried out with time step of (1×10^{-4} sec.), PIMPLE loop using (`nCorrectors` = 3) to the solver scheme, and two alpha correctors (`nAlphaCorr` = 2) for mass equation. The alpha correction was enable on last PIMPLE loop. The gravity forces and another interfacial forces were neglected. The drag force of the disperse and the continuous phases used was a constant value of $Cd = 0,41$ and the regime variable number computed with Schiller-Naumman model.

Two different meshes of 20 and 100, uniform lineal volume controls were used. Figure 12 shows the numerical solutions for the dispersed velocity along the pipe like as the Schiller-

Naumman drag coefficient.

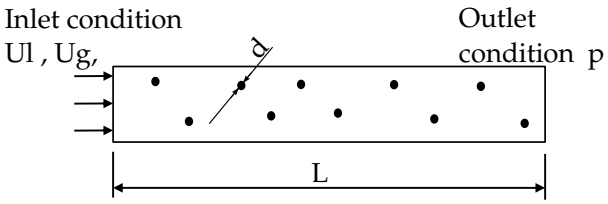

Figure 10: Dispersed phase velocity and S-N drag model

Table 2: Details of Particle Transport Problem

Geometric details			
Length (m)		2	
Diameter (m)		1	
Initial Conditions		**Boundary Conditions**	
α	1×10^{-5}	α	1×10^{-5}
$u_{continous}(m/s)$	5	$u_{inlet,l}(m/s)$	5
$u_{dispersed}(m/s)$	1	$u_{inlet,g}(m/s)$	1

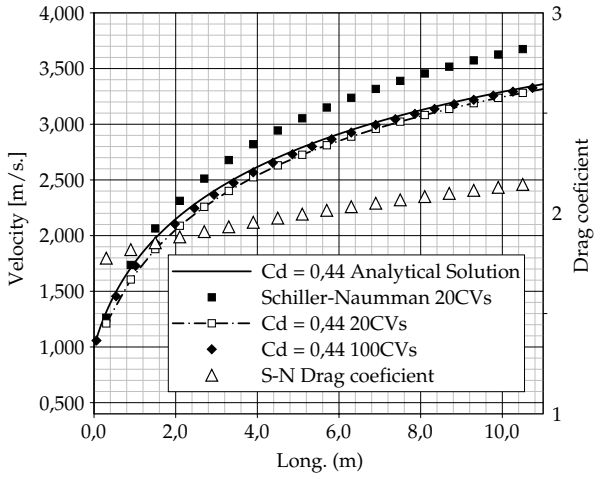

Figure 11: Dispersed phase velocity and S-N drag model

4.3 Evaporation model test

For the validation of the evaporation model capabilities, the Bartolomej (Bartolomej and Chanturiya, 1967) test was solved. The continuous temperature field T_l, the U_l and U_g velocities, and the void fraction α in the pipe was loaded from steady state results obtained in Appendix. The CFD script to approach the RPI parameters and the vapor mass flow generated on the wall was implemented in **octave**. The code loads the above mentioned variables on the near-wall cells and running the evaporation model in each one of these cells.

Figure 12 shows the comparison between the obtained results and CFX model described on Appendix. To achieve the good agreement showed, the evaporation models were slightly modified and it is explained on Appendix section.

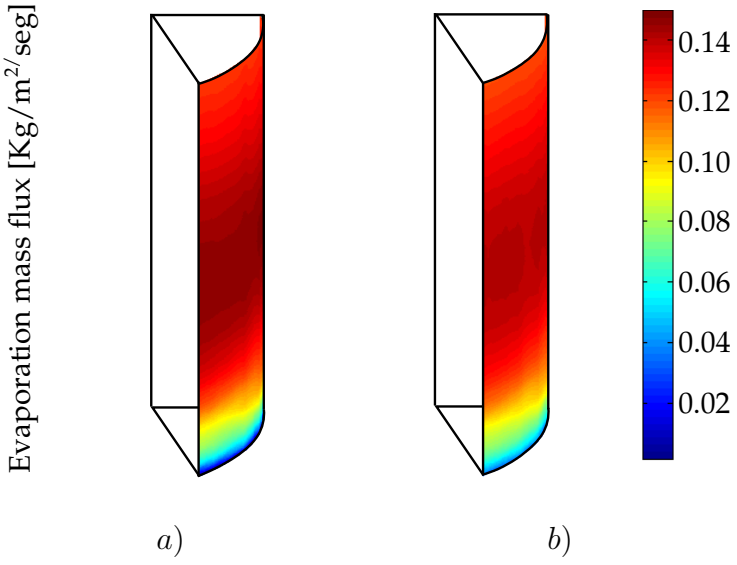

Figure 12: Evaporation mass flow rate on heated wall: a) Developed model, b) CFX

5 CONCLUSIONS

A one-dimensional two-phase Euler model is proposed in this paper. A depth analysis about mass and momentum interfacial iteration was carried out for the most used empirical correlations. This correlations performs well for dispersed bubbly regime presented on subcooled evaporation. The governing equations for the two-phase model are based on Finite Volume Methods and implemented in OpenFOAM® suit. The **Octave-of** model was successfully implemented based on **twoPhaseEulerFoam** solver. The results presented reveals a good agreement respect to experimental dates. Friction looses models are required to recover the misses of transversal shear stress in one-dimensional domains. Finally, we present a detailed description of the evaporation and condensation model for subcooled flows. This CFD approach developed by Kurul and Podowski (Kurul and Podowski, 1991) was implemented and compared with experimental results. Regarded to the complete implementation of RPI model on one-dimensional solver a relationship for the near-wall temperature is needed. Predict the temperature close to the wall will be treated in following papers.

Three benchmarks test was solved to validate the model. The water faucet shows the influence of the gravity force in the numerical resolution. The drag force influence on the disperse momentum equation has been studied on a particles transport test. The subcooled boiling evaporation rate was tested in a heated pipe where compare the local parameters with CFX results.

More benchmark tests must be tested in the future including a complete analysis of stability.

REFERENCES

Ansys C. Solver theory guide. *ANSYS Inc., Southpointe*, 2006.

Antal S., Lahey Jr R., and Flaherty J. Analysis of phase distribution in fully developed laminar bubbly two-phase flow. *International Journal of Multiphase Flow*, 17(5):635–652, 1991.

Bartolomej G. and Chanturiya V. Experimental study of true void fraction when boiling subcooled water in vertical tubes. *Thermal Engineering*, 14(2):123–128, 1967.

BOREE J., CARAMAN N., ISHIMA T., FANOUILLERE P., and FLOUR I. Influence du chargement massique dans un ecoulement etabli diphasique en tube. ????

Ceumern-Lindenstjerna W. Bubble departure diameter and release frequencies during nucleate pool boiling of water and aqueous sodium chloride solutions. *Heat Transfer Boiling, Hemisphere, New York*, pages 53–75, 1997.

Chisholm D. and Laird A. Two-phase flow in rough tubes. *Trans. ASME*, 80(2):276–286, 1958.

Claxton K., Collier J., and Ward J. *HTFS Correlations for Two-phase Pressure Drop and Void Fraction in Tubes*. Heat Transfer and Fluid Flow Service, 1972.

Clift R., Grace J., Weber M., and Clift R. *Bubbles, drops, and particles*, volume 3. Academic press New York, 1978.

Cordes G. E. truckenbrodt, stromungsmechanik. grundlagen und technische anwendungen. berlin/heidelberg/new york 1968. springer-verlag. preis geb. dm 69,. *ZAMM-Journal of Applied Mathematics and Mechanics/Zeitschrift fur Angewandte Mathematik und Mechanik*, 49(11):704–704, 1969.

Del Valle V. and Kenning D. Subcooled flow boiling at high heat flux. *International Journal of Heat and Mass Transfer*, 28(10):1907–1920, 1985.

Drew D. and Lahey Jr R. Rge virtual mass and lift force on a sphere in rotating and straining inviscid flow. *International Journal of Multiphase Flow*, 13(1):113–121, 1987.

Enwald H., Peirano E., and Almstedt A. Eulerian two-phase flow theory applied to fluidization. *International Journal of Multiphase Flow*, 22:21–66, 1996.

Evje S. and Fjelde K. Hybrid flux-splitting schemes for a two-phase flow model. *Journal of Computational Physics*, 175(2):674–701, 2002.

Ferziger J. and Perić M. *Computational methods for fluid dynamics*, volume 3. Springer Berlin etc, 1999.

Ghiaasiaan S. *Two-phase flow, boiling and condensation in conventional and miniature systems*. Cambridge Univ Pr, 2008.

Gidaspow D. *Multiphase flow and fluidization: continuum and kinetic theory descriptions*. Academic Pr, 1994.

Guide O. Openfoam-the open source cfd toolbox-programmer'sguide. 2004.

Hewitt G. *Multiphase fluid flow and pressure drop, heat exchanger design handbook*. 1983.

Hwang Y. Upwind scheme for non-hyperbolic systems. *Journal of Computational Physics*, 192(2):643–676, 2003.

Ishii M. and Hibiki T. Thermo-fluid dynamics of two-phase flow. 2006: Springer science. ????

Ishii M. and Zuber N. Drag coefficient and relative velocity in bubbly, droplet or particulate flows. *AIChE Journal*, 25(5):843–855, 1979.

Issa R. and Kempf M. Simulation of slug flow in horizontal and nearly horizontal pipes with the two-fluid model. *International journal of multiphase flow*, 29(1):69–95, 2003.

Jasak H. Error analysis and estimation for the finite volume method with applications to fluid flows. *Direct*, 1000(June), 1996.

Jens W. and Lottes P. Analysis of heat transfer, burnout, pressure drop and density date for

high-pressure water. Technical Report, Argonne National Lab., 1951.

Krepper E., Končar B., and Egorov Y. Cfd modelling of subcooled boilingâĂŤconcept, validation and application to fuel assembly design. *Nuclear Engineering and Design*, 237(7):716–731, 2007.

Kurul N. and Podowski M. On the modeling of multidimensional effects in boiling channels. In *Proceedings of the 27th National Heat Transfer Conference*. 1991.

Lerchl G. and Austregesilo H. The athlet code documentation package. *UserâĂŹs Manual, GRS-P*, 1, 1995.

Levy S. Forced convection subcooled boiling–prediction of vapor volumetric fraction. *International Journal of Heat and Mass Transfer*, 10(7):951–965, 1967.

Morales-Ruiz S., Rigola J., Rodriguez I., and Oliva A. Numerical resolution of the liquid-vapour two-phase flow by means of the two-fluid model and a pressure based method. *International Journal of Multiphase Flow*, 2012.

Moukalled F. and Darwish M. A comparative assessment of the performance of mass conservation-based algorithms for incompressible multiphase flows. *Numerical Heat Transfer: Part B: Fundamentals*, 42(3):259–283, 2002.

Pellacani F., Mestre S., Vicent S., and Juan R. Cfd modeling of isothermal and non-isothermal bubbly flow in vertical condition using ansys cfx 12. ????

Ransom V. and Mousseau V. Convergence and accuracy of the relap5 two-phase flow model. In *Proceedings of the ANS International Topical Meeting on Advances in Mathematics, Computations, and Reactor Physics*. 1991.

Saha P. and Zuber N. Point of net vapor generation and vapor void fraction in subcooled boiling. Technical Report, Georgia Inst. of Technology, Atlanta, 1974.

Schiller L. and Naumann A. Uber die grundlegenden berechnungen bei der schwerkraftaufbereitung. *Ver. Deut. Ing*, 77(318-320):33, 1933.

Shieh A., Ramsom V., and Krishnamurty R. Relap5/mod3 code manual, volume 6: Validation of numerical techniques. *Informe Técnico NUREG/CR-5535/Rev*, 3, ????

Thom J. Boiling in sub-cooled water during flow up heated tubes or annuli. *Proc. Inst. Mech. Engrs.*, 180(3):226, 1966.

Tolubinsky V. and Kostanchuk D. Vapour bubbles growth rate and heat transfer intensity at subcooled water boiling. In *Proceedings of the 4th International Heat Transfer Conference*, volume 5. 1970.

Unal H. Maximum bubble diameter, maximum bubble-growth time and bubble-growth rate during the subcooled nucleate flow boiling of water up to 17. 7 mn/sq m. *International Journal of Heat and Mass Transfer*, 19:643–649, 1976.

Versteeg H. and Malalasekera W. *An introduction to computational fluid dynamics: the finite volume method*. Prentice Hall, 2007.

Wallis G. One-dimensional two-phase flow, mcgraw hill. *New York*, 1969.

Wolfert K., Burwell M., and Enix D. Non-equilibrium mass transfer between liquid and vapour phases during depressurization processes in transient two-phase flow. In *Proc. of 2nd CSNI Specialists Meeting, Paris*, volume 1. 1978.

6 APPENDIX

6.1 Bartolomej test benchmark

The Bartolomej experiment was performed in a 2 m long heated tube with diameter of $15,4$ mm was selected. The heat flux on the wall was $3,8 \times 10^5$ W/m^2. The mass flow was 900 Kg/sec/m^2 and the temperature inlet condition $T_{sub} = 58,2$K. An outlet pressure of 4.5MPa. The model was represented by a 1/6 of the total section. Simulations were carried out using a 3D grid of 87450 cells developed completely in CFX. This code is based on the Finite Volume Method. Use a semi-implicit arrangement for the pressure linked equation (SIMPLE algorithm) to the pressure-velocity coupling. Shear stress transport turbulence model was used for the continuous phase. High order discretization scheme for momentum equation and first order upwind for turbulence quantities was used here (Ansys, 2006). The following models were used follow the Krepper (Krepper et al., 2007) recommendations: The Sato model for the bubble induced turbulence, the Grace model of the interfacial drag (Clift et al., 1978), Tolubinsky model for the bubble departure diameter. The Non-drag forces was modeled by: Tomiyama model for lift forces, Equation 23 for Virtual mass forces where $C_{VM} = 0,5$, Favre-averaged turbulent model for the turbulent dispersion force and Antal approach (Antal et al., 1991) for the wall lubrication force (with Antal coefficient: $C1 = -0,025$ and $C2 = 0,075$).

Figure 13 shows the water temperature in the bulk and the void fraction distribution. This sumariezed results show the good agreement for CFD models. The results was compared to an

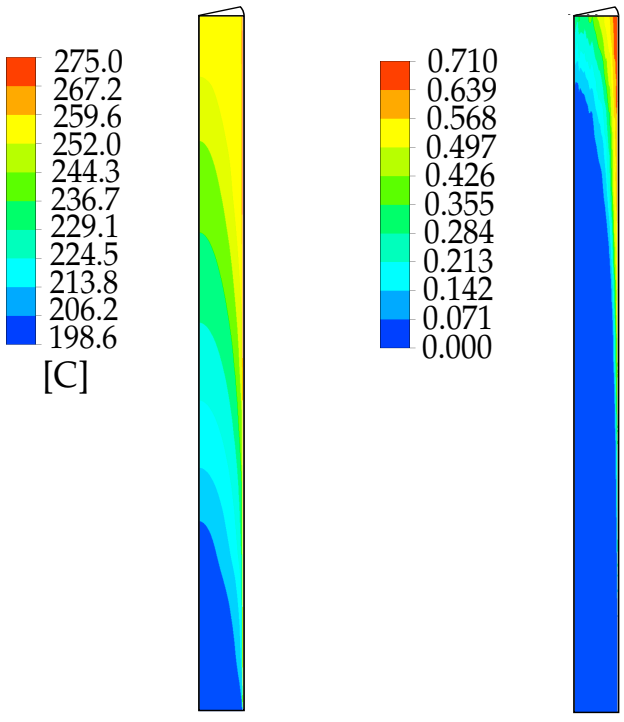

Figure 13: Numerical solution of Bartolomej test: a) Temperature and b) Void fraction distribution.

advanced code for simulation of design basis in light water reactors named ATHLET (Lerchl and Austregesilo, 1995). This code developed by Gesellschaft fur Anlagenund Reaktorsicherheit (GRS) is a one-dimensional, two-phase fluid-dynamics models based on a five-equation model. The results are showed on figure 14. The void fraction prediction on the outlet surface presents a good agreement respect to experimental results. The axial distribution of void fraction is slightly different to experimental results. This might lie in interfacial momentum correlations.

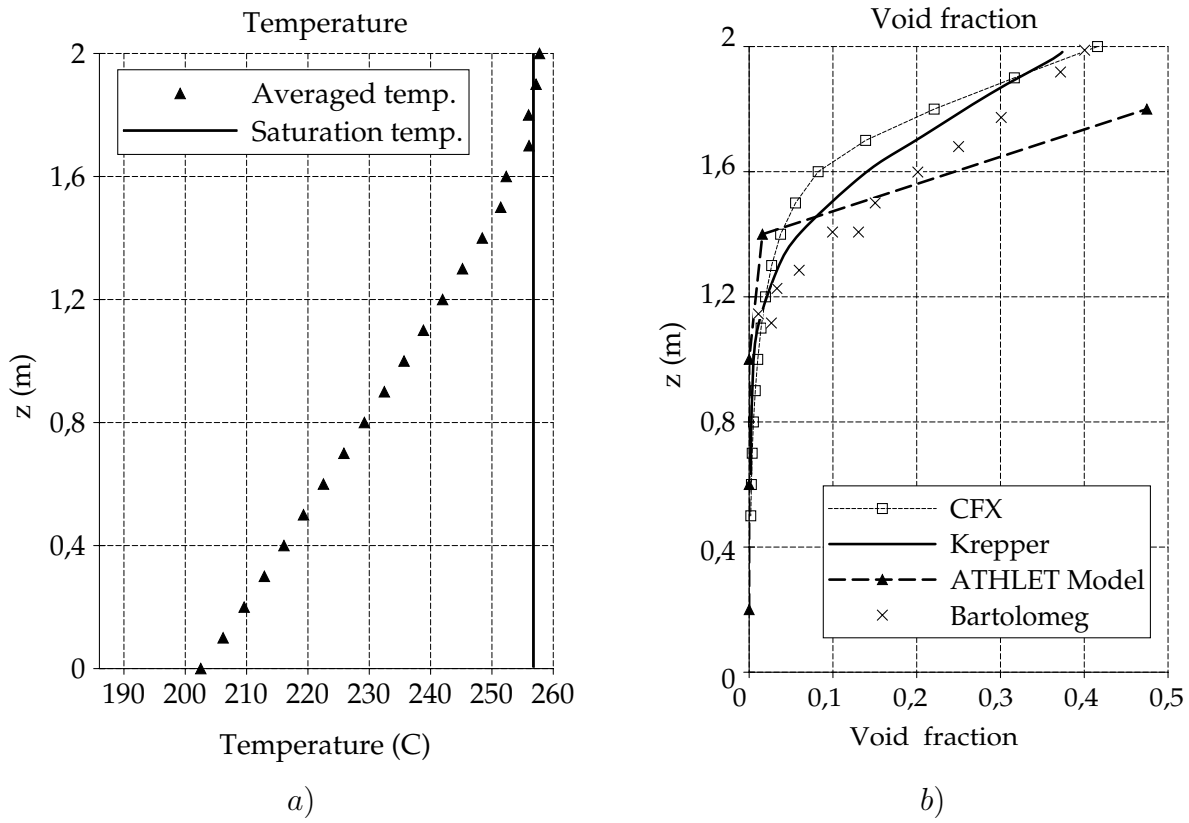

Figure 14: Numerical solution of Bartolomej test: Averaged a) Temperature and b) Void fraction distribution.